Available online at www.sciencedirect.com
ScienceDirect
Mathematics and Computers in Simulation 82 (2011) 220–233
MATHEMATICS AND COMPUTERS IN SIMULATION
www.elsevier.com/locate/matcom

Solving convection-diffusion-reaction equation by adaptive finite volume element method

P. Theeraek [a], S. Phongthanapanich [b], P. Dechaumphai [a,*]

[a] *Department of Mechanical Engineering, Faculty of Engineering, Chulalongkorn University, Patumwan, Bangkok 10330, Thailand*
[b] *Department of Mechanical Engineering Technology, College of Industrial Technology, King Mongkut's University of Technology North Bangkok, Bangkok 10800, Thailand*

Received 16 August 2010; received in revised form 17 March 2011; accepted 7 June 2011
Available online 12 July 2011

Abstract

A finite volume element method is combined with an adaptive meshing technique to solve the two-dimensional unsteady convection-diffusion-reaction equation. The finite volume method is used to derive the discretized equations while concept of the finite element technique is applied to determine the gradient quantities at cell faces. Second-order accuracy in both space and time are achieved by applying the Taylor's series expansion along the local characteristic lines. An adaptive meshing technique is applied to further improve the solution accuracy, and to minimize the computational time and computer memory requirement. The efficiency of the adaptive finite volume element method is evaluated by the examples of pure-convection, convection-diffusion, convection-reaction, and diffusion-reaction problems.

Keywords: Convection-diffusion-reaction equation; Finite volume element method; Adaptive meshing technique

1. Introduction

Numerical simulation for predicting the transport phenomena governed by the unsteady convection-diffusion-reaction equation is difficult due to the convection term. The flow behaviors usually contain steep gradients that require special treatment of numerical schemes. Most of the classical schemes suffer from the spurious oscillations, otherwise yield excessive numerical dispersion [9,20]. During the past decade, several stabilizing schemes have been developed for solving such equation. These schemes include the upwind-based methods [11,13], the characteristic Galerkin method [4,21], the Galerkin projected residual method [3], the improved stabilization parameter on the Petrov–Galerkin method and on the multiscale method [7,19], the Taylor–Galerkin algorithm [14], etc. The upwind-based methods have been employed widely for analyzing strongly convective flow. The characteristics Galerkin method based on the Taylor's series expansion is an attractive one due to its simple implementation that can be written in a fully explicit form for obtaining solution. Other schemes with high-resolution have also been investigated such as those proposed in Refs. [8,10,12]. At present, development of new numerical schemes for accurate solution of the convection-diffusion-reaction equation is still needed.

* Corresponding author. Tel.: +66 2 218 6621; fax: +66 2 218 6621.
E-mail address: fmepdc@eng.chula.ac.th (P. Dechaumphai).

0378-4754/$36.00 © 2011 IMACS. Published by Elsevier B.V. All rights reserved.
doi:10.1016/j.matcom.2011.06.002

Computational techniques for solving the hyperbolic equation are generally classified into the explicit and implicit (or semi-implicit) methods. The explicit method is popular because it is simple and requires less computational effort. However, the method is constrained by the CFL condition in order to stabilize the spatial error from growing without bound. On the other hand, the implicit method provides more stable solution but a large time step may not be used because the solution accuracy degrades with time. The inversion of the coefficient matrix is another weakness of the latter method since it is a time consumable process. Furthermore, a large block of memory is required for the coefficient matrix formation.

In this paper, the finite volume element method [17,18] is further investigated and presented. A cell-centered finite volume method is used to discretize the two-dimensional unsteady convection-diffusion-reaction equation on triangular meshes. The midpoint quadrature is applied for both the spatial and temporal flux integral terms, while second-order accurate unknown quantities at the cell faces are determined by using the Taylor's series expansion. An explicit scheme is achieved by expanding the temporal gradient along the local characteristics and using the finite element concept to determine the gradient quantities at the cell faces. An adaptive meshing technique is implemented to further improve the solution accuracy by refining meshes in the region of high solution gradients. Coarse meshes are constructed in the other regions to reduce the computational time and computer memory. The presentation of this paper starts from the explanation of the theoretical formulation and adaptive meshing technique in Sections 2–4, respectively. Performance of the combined method is examined by using five examples. These examples are: (1) mixing of hot with cold front, (2) boundary layer flow, (3) oblique inflow convection-reaction, (4) corner layer problem, and (5) triangular wave flow problem.

2. Governing equation and finite volume element formulation

The governing equation for the two-dimensional unsteady convection-diffusion-reaction equation is,

$$\frac{\partial \phi}{\partial t} + \vec{\nabla} \cdot (\vec{v}\phi - \epsilon \vec{\nabla}\phi) + \kappa\phi = q \tag{1}$$

where ϕ is the unknown scalar quantity, $\vec{v} = v_x\vec{i} + v_y\vec{j}$ is the given convective velocity, $\epsilon \geq 0$ is the diffusivity parameter, κ is the reaction coefficient, and $q = q(\vec{x}, t)$ is the prescribed source term. Eq. (1) is defined for the spatial domain $\vec{x} \in \Omega$ where $\Omega \subset R^2$ and the time interval of $t \in (0, T)$ with $T > 0$. The initial condition is given by $\phi(\vec{x}, 0) = \phi_0(\vec{x})$.

The finite volume element technique is proposed herein for solving the unsteady convection-diffusion-reaction equation. The discretization is based on the cell-centered method for which the non-overlapping triangular control volumes, $\Omega_i \in \Omega$, $i = 1, 2, \ldots, N$, are placed over the computational domain such that $\Omega = \bigcup_{i=1}^{N} \Omega_i$, $\Omega_i \neq 0$, and $\Omega_i \cap \Omega_j = \varnothing$, if $i \neq j$. The governing equation is subject to the boundary conditions

$$\phi = g_D \quad \text{on} \quad \partial\Omega_D, \tag{2a}$$

$$\epsilon \frac{\partial \phi}{\partial \vec{n}} = g_N \quad \text{on} \quad \partial\Omega_N \tag{2b}$$

with $\partial\Omega = \partial\Omega_D \cup \partial\Omega_N$ and $\partial\Omega_D \cap \partial\Omega_N = \varnothing$. Eq. (1) is integrated over the control volume Ω_i and in the time interval (t^n, t^{n+1}) as,

$$\int_{\Omega_i} \int_{t^n}^{t^{n+1}} \left(\frac{\partial \phi}{\partial t} + \vec{\nabla} \cdot (\vec{v}\phi - \epsilon \vec{\nabla}\phi) + \kappa\phi - q \right) dt\, d\vec{x} = 0 \tag{3}$$

The approximations to the cell average of ϕ over control volume Ω_i at time t^n and t^{n+1} are represented by,

$$\phi_i^n = \frac{1}{meas(\Omega_i)} \int_{\Omega_i} \phi(\vec{x}, t^n) d\vec{x}, \tag{4a}$$

and

$$\phi_i^{n+1} = \frac{1}{meas(\Omega_i)} \int_{\Omega_i} \phi(\vec{x}, t^{n+1}) d\vec{x} \tag{4b}$$

where $meas(\Omega_i)$ is the area of cell i. Temporal integration of the transient term and application of the divergence theorem for the convection-diffusion term yield,

$$\phi_i^{n+1} = \phi_i^n - \frac{1}{meas(\Omega_i)} \int_{t^n}^{t^{n+1}} \int_{\partial\Omega_i} \vec{n}_i(\upsilon) \cdot \left[\vec{v}(\upsilon)\phi(\vec{x},t) - \epsilon\vec{\nabla}\phi(\upsilon,t)\right] d\upsilon\, dt$$
$$- \frac{1}{meas(\Omega_i)} \left[\int_{\Omega_i}\int_{t^n}^{t^{n+1}} \kappa\,\phi(\vec{x},t)dt\, d\vec{x} - \int_{\Omega_i}\int_{t^n}^{t^{n+1}} q(\vec{x},t)dt\, d\vec{x}\right] \tag{5}$$

where $\vec{n}_i(\upsilon)$ is the outward unit normal vector to the cell face, $\partial\Omega_i$.

For an arbitrary triangular control volume, the flux integral over $\partial\Omega_i$ appearing on the right-hand side of Eq. (5) could be approximated by summation of the fluxes passing through the three adjacent cell faces. By applying the midpoint quadrature integration rule for both the spatial and temporal domains, the flux integral over $\partial\Omega_i$ in Eq. (5) is approximated by,

$$\int_{t^n}^{t^{n+1}} \int_{\partial\Omega_i} \vec{n}_i(\upsilon) \cdot \left[\vec{v}(\upsilon)\phi(\vec{x},t) - \epsilon\vec{\nabla}\phi(\upsilon,t)\right] d\upsilon\, dt = \Delta t \sum_{j=1}^{3} |\Gamma_{ij}|\vec{n}_{ij} \cdot \left[\vec{v}_{ij}\phi_{ij}(t^{n+1/2}) - \epsilon\vec{\nabla}\phi_{ij}(t^{n+1/2})\right] \tag{6}$$

where subscript ij indicates the quantity evaluated at midpoint of the cell face between the two adjacent cells, Ω_i and Ω_j. The segment of boundary, Γ_{ij}, is defined by $\partial\Omega_i = \bigcup_{j=1}^{3}\Gamma_{ij}$ and $\Gamma_{ij} = \partial\Omega_i \cap \partial\Omega_j$. The velocity vector, $\vec{v}_{ij}$, and the unknown quantity at the half time step, $\phi_{ij}(t^{n+1/2})$, are also evaluated at midpoint of each cell face. It should be noted that, for simplicity, $\vec{\nabla}\phi_{ij}(t^{n+1/2})$ is approximated by $\vec{\nabla}\phi_{ij}(t^n)$ throughout this paper.

Integration of the reaction and source terms could be approximated by the cell average over the control volume and the midpoint quadrature integration rule in time domain as,

$$\int_{\Omega_i}\int_{t^n}^{t^{n+1}} \kappa\,\phi(\vec{x},t)dt\, d\vec{x} = meas(\Omega_i)\Delta t\,\kappa\,\phi_i(t^{n+1/2}) \tag{7}$$

$$\int_{\Omega_i}\int_{t^n}^{t^{n+1}} q(\vec{x},t)dt\, d\vec{x} = meas(\Omega_i)\Delta t\, q_i(t^{n+1/2}) \tag{8}$$

By substituting Eqs. (6)–(8) into Eq. (5), an explicit finite volume scheme for solving Eq. (1) is obtained as,

$$\phi_i^{n+1} = \phi_i^n - \frac{\Delta t}{meas(\Omega_i)} \left[\sum_{j=1}^{3} |\Gamma_{ij}|\vec{n}_{ij} \cdot \left(\vec{v}_{ij}\phi_{ij}^{n+1/2} - \epsilon\vec{\nabla}\phi_{ij}^n\right)\right] - \Delta t\left(\kappa\,\phi_i^{n+1/2} - q_i^{n+1/2}\right) \tag{9}$$

where the quantities at time $t^{n+1/2}$ are defined by $\phi_{ij}^{n+1/2} = \phi_{ij}(t^{n+1/2})$, $\phi_i^{n+1/2} = \phi_i(t^{n+1/2})$, and $q_i^{n+1/2} = q_i(t^{n+1/2})$. The gradient quantity at time t^n is defined by $\vec{\nabla}\phi_{ij}^n = \vec{\nabla}_{ij}\phi(t^n)$. The quantities at the half time step, $\phi_{ij}^{n+1/2}$ and $\phi_i^{n+1/2}$, are of second-order and approximated by applying Taylor's series expansion as,

$$\phi_{ij}^{n+1/2} = \phi_i^n + (\vec{x}_{ij} - \vec{x}_i) \cdot \vec{\nabla}\phi_i^n + \frac{\Delta t}{2}\frac{\partial\phi_i^n}{\partial t} \tag{10}$$

$$\phi_i^{n+1/2} = \phi_i^n + \frac{\Delta t}{2}\frac{\partial\phi_i^n}{\partial t} \tag{11}$$

To obtain an explicit scheme, the temporal derivative terms in Eqs. (10) and (11) are determined by using the concept of local expansion of the unknown along its characteristics. Hence, the reconstruction of transport quantities according to the upwind direction can be written as,

$$\phi_{ij}^{n+1/2} = \begin{cases} \phi_i^n + (\vec{x}_{ij} - \vec{x}_i) \cdot \vec{\nabla}\phi_i^n - \dfrac{\Delta t}{2}(\vec{v}_i \cdot \vec{\nabla}\phi_i^n), \vec{v}_{ij} \cdot \vec{n}_{ij} \geq 0 \\ \phi_j^n + (\vec{x}_{ij} - \vec{x}_j) \cdot \vec{\nabla}\phi_j^n - \dfrac{\Delta t}{2}(\vec{v}_j \cdot \vec{\nabla}\phi_j^n), \vec{v}_{ij} \cdot \vec{n}_{ij} < 0 \end{cases} \tag{12}$$

$$\phi_i^{n+1/2} = \begin{cases} \phi_i^n - \dfrac{\Delta t}{2}(\vec{v}_i \cdot \vec{\nabla}\phi_i^n), \vec{v}_{ij} \cdot \vec{n}_{ij} \geq 0 \\ \phi_j^n - \dfrac{\Delta t}{2}(\vec{v}_j \cdot \vec{\nabla}\phi_j^n), \vec{v}_{ij} \cdot \vec{n}_{ij} < 0 \end{cases} \tag{13}$$

In this paper, the concept of finite element method is applied to determine the gradient quantities. The gradient at the center of control volume, $\vec{\nabla}\phi_i^n$, is determined by the weighted residuals method [6,22] and is assumed to be linearly distributed over cell Ω_i,

$$\vec{\nabla}\phi_i^n = \sum_{k=1}^{3} N_k(\vec{x})\vec{\nabla}\phi_k^n \tag{14}$$

where $N_k(\vec{x})$ denotes the linear interpolation functions for the triangular cell and $k = 1, 2, 3$ represent the control volume vertices. By applying the standard Galerkin method and the Gauss's theorem to Eq. (14), the gradient quantities at a grid point are obtained as,

$$\vec{\nabla}\phi_{J,i}^n = M^{-1}\left[\int_{\partial\Omega_i} \vec{n}_i(\upsilon) N_J(\upsilon)\phi_i^n d\upsilon - \int_{\Omega_i} \frac{\partial N_J(\upsilon)}{\partial \vec{x}}\phi_i^n d\vec{x}\right] \tag{15}$$

where M is the lumped mass matrix and $\vec{\nabla}\phi_{J,i}^n$ are the contributions of the gradient quantities in the control volume Ω_i to the gradient quantities at the grid point J. In order to determine the total gradient quantities at the grid point J, Eq. (15) is applied to all the volumes surrounding it such that,

$$\vec{\nabla}\phi_J^n = \sum_{i=1}^{NV} \vec{\nabla}\phi_{J,i}^n \tag{16}$$

where NV is the number of the surrounding triangular cells. The gradient quantities at the cell faces, $\vec{\nabla}\phi_{ij}^n$, is then computed by applying the midpoint quadrature integration rule along the edge that connects grid points I and J.

To ensure the stability of an explicit scheme on a triangular mesh, the CFL-like stability criterion must be fulfilled. In this paper, the permissible time step within each cell is determined from

$$\Delta t = C \min_i \left(\frac{(meas(\Omega_i))^{1/2}}{\max_{j=1,2,3}|\vec{v}_{n,ij}|}, \frac{|\Gamma_i^c|^2}{2\epsilon} \right) \tag{17}$$

where $\vec{v}_{n,ij}$ is the normal velocity at Γ_{ij}, Γ_i^c is the characteristic length of cell i, and $0 < C \leq 1$.

3. One-dimensional numerical analysis

In this section, a numerical analysis of the one-dimensional homogeneous convection-diffusion equation is presented. For simplicity, the order of accuracy and stability of the explicit numerical scheme given by Eq. (18) will be analyzed on a uniform one-dimensional grid cell, $meas(\Omega_i) = \Delta x$. The one-dimensional homogeneous convection-diffusion equation is

$$\frac{\partial \phi}{\partial t} + \frac{\partial}{\partial x}\left(a\phi - \epsilon\frac{\partial \phi}{\partial x}\right) = 0 \tag{18}$$

where a is a given velocity. The numerical equation for the ith cell, $meas(\Omega_i) \in (x_{i-1/2}, x_{i+1/2})$, may be written as

$$\phi_i^{n+1} = \phi_i^n - \frac{a\Delta t}{\Delta x}\left(\phi_{i+1/2}^{n+1/2} - \phi_{i-1/2}^{n+1/2}\right) + \frac{\epsilon\Delta t}{\Delta x}\left(\left.\frac{\partial \phi}{\partial x}\right|_{i+1/2}^{n} - \left.\frac{\partial \phi}{\partial x}\right|_{i-1/2}^{n}\right) \tag{19}$$

By using the one-dimensional linear interpolation function, the gradient quantities at the cell faces $i - 1/2$ and $i + 1/2$ are

$$\left.\frac{\partial \phi}{\partial x}\right|_{i-1/2}^{n} = \frac{1}{\Delta x}\left(\phi_i^n - \phi_{i-1}^n\right) \tag{20a}$$

$$\left.\frac{\partial\phi}{\partial x}\right|_{i+1/2}^{n} = \frac{1}{\Delta x}\left(\phi_{i+1}^{n} - \phi_{i}^{n}\right) \tag{20b}$$

Similarly, the gradient quantity at cell-centered of $|\Omega_i|$ is

$$\left.\frac{\partial\phi}{\partial x}\right|_{i}^{n} = \frac{1}{2\Delta x}\left(\phi_{i+1}^{n} - \phi_{i-1}^{n}\right) \tag{21}$$

By substituting these expressions into the right-hand side of Eq. (19)

$$\phi_i^{n+1} = \phi_i^n - \frac{R}{4}\left(\phi_{i+1}^n + 3\phi_i^n - 5\phi_{i-1}^n + \phi_{i-2}^n\right) + \frac{R^2}{4}\left(\phi_{i+1}^n - \phi_i^n - \phi_{i-1}^n + \phi_{i-2}^n\right) + r\left(\phi_{i+1}^n - 2\phi_i^n + \phi_{i-1}^n\right) \tag{22}$$

where $R = (a\Delta t)/(\Delta x)$ and $r = (\epsilon\Delta t)/((\Delta x)^2)$, are the cell Courant number and the cell diffusion parameter, respectively. The truncation error analysis by using the Taylor series expansion on Eq. (22) at $(x_n, t^n) = (i, n)$ shows that the accuracy is of order $O(\Delta t^2, \Delta t\Delta x, \Delta x^2)$.

To analyze the stability of the numerical scheme, the discrete Fourier transform is applied to Eq. (22), term by term, to obtain the amplification factor $G(\theta)$ as

$$\begin{aligned} G(\theta) = \frac{\hat{\phi}^{n+1}}{\hat{\phi}^n} &= \left[1 - R(\cos(\theta) - 1)^2 - \frac{R^2}{2}\sin^2(\theta) + 2r(\cos(\theta) - 1)\right] \\ &\quad - I(R\sin(\theta))\left[(3 - \cos(\theta)) - \frac{R}{2}(1 - \cos(\theta))\right] \end{aligned} \tag{23}$$

where θ is a phase angle. For a stable solution, the modulus of $G(\theta)$ must be bounded for all values of θ ($|G(\theta)|^2 \le 1$), i.e.,

$$\begin{aligned} |G(\theta)|^2 = (\cos(\theta) - 1)&\left[\left(\frac{R^2}{2} - 2R^3 + 2R^2 r\right)(\cos^2(\theta) - 1) + R^2(2\cos^2(\theta) + \cos(\theta) - 9) - 4Rr(\cos(\theta) - 1)^2\right. \\ &\left. + (4r^2 - 2R)(\cos(\theta) - 1) + 4r\right] + 1 \end{aligned} \tag{24}$$

By differentiating Eq. (24) with respect to θ and setting the derivative to be zero, the critical points are at $\theta = 0, \pm\pi$. The values of $|G(\theta)|$ at these points are

$$\begin{aligned} |G(0)| &= 1 \\ |G(\pm\pi)| &= |4(R + r) - 1| \end{aligned} \tag{25}$$

For $|G(\pm\pi)|$ to be bounded by one, the numerical scheme is conditionally stable when $0 \le R + r \le (1/2)$. Such condition implies that $|G(\theta)| \le 1 + C\Delta t$, where $C > 0$. The numerical scheme satisfies the von Neumann condition, thus the scheme is stable. However, it should be noted that the stability condition is restrictive. The CFL-like condition as described by Eq. (17), which is obtained by applying the discrete Fourier transform to the convection and diffusion parts separately, is stable with a large time step. Such stability condition has been tested by using many numerical examples as will be presented in the following section.

To ensure that the proposed explicit scheme converges and does not produce global oscillation, the time step is determined from the CFL condition given by Eq. (17). In addition, to reduce the local oscillation, the upwind technique according to Eq. (10) is used for discretizing the convection term. By following the one-dimensional analysis above, an implicit diffusion term $((a^2\Delta t)/2)((\partial^2\phi)/(\partial x^2))$ is generated which is essential for the upwind scheme. However, some local oscillations still remain because the Taylor's series is used to formulate the higher-order reconstruction of the unknown quantities at the cell faces. To eliminate such oscillation, a less accurate solution is obtained by writing the unknown quantities at the cell faces as $\phi_{ij} = \phi_i$.

4. Adaptive meshing technique

The concept of the adaptive meshing technique is to generate an entirely new mesh based on the solution obtained from an earlier mesh [5,15]. The new mesh consists of small elements in the regions with large change in solution gradients and larger elements in the other regions where the changes in solution gradients are small. The adaptive meshing procedure employed in this paper is based on the advancing front technique for which the grid points are firstly generated along the outer domain boundary. Triangular elements are then constructed from these grid points and gradually propagate into the domain interior. The mesh construction is complete when the domain interior is fulfilled with all triangular elements. To determine proper element sizes at different locations in the flow field, the solid-mechanics concept for finding the principal stresses from a given state of stresses at a point is employed. The second derivatives of the unknown quantity ϕ with respect to global coordinates $\vec{x}$ can be computed in the principal directions $\vec{X}$ as,

$$\begin{bmatrix} \dfrac{\partial^2\phi}{\partial x^2} & \dfrac{\partial^2\phi}{\partial x\partial y} \\ \dfrac{\partial^2\phi}{\partial x\partial y} & \dfrac{\partial^2\phi}{\partial y^2} \end{bmatrix} \Rightarrow \begin{bmatrix} \dfrac{\partial^2\phi}{\partial X^2} & 0 \\ 0 & \dfrac{\partial^2\phi}{\partial Y^2} \end{bmatrix} \tag{26}$$

The second derivatives of the unknown quantity ϕ with respect to coordinates $\vec{x}$ are determined by using the concept of weighted residuals. For example, to determine $(\partial^2\phi)/(\partial x^2)$, the computed solution ϕ_i, is assumed to vary linearly over cell Ω_i as

$$\phi_i = \sum_{k=1}^{3} N_k(\vec{x})\phi_k \tag{27}$$

where $N_k(\vec{x})$ denotes the linear interpolation functions for the triangular cell and $k = 1, 2, 3$ are the control volume vertices. By applying the standard Galerkin method, the first derivative can be derived and determined from,

$$\left.\frac{\partial\phi}{\partial x}\right|_{J,i} = M^{-1}\int_{\Omega_i} N_J\, d\vec{x}\, \left.\frac{\partial\phi}{\partial x}\right|_i \tag{28}$$

where M is the lumped mass matrix and $((\partial\phi)/(\partial x))|_{J,i}$ is the contribution of the first derivative quantity at the grid point J. By applying the same procedure, the second derivative is,

$$\left.\frac{\partial^2\phi}{\partial x^2}\right|_{J,i} = M^{-1}\int_{\Omega_i} N_J\, d\vec{x}\, \left.\frac{\partial^2\phi}{\partial x^2}\right|_i \tag{29}$$

Then, the second derivative at the grid point J is determined from,

$$\left.\frac{\partial^2\phi}{\partial x^2}\right|_J = \sum_{i=1}^{NV} \left.\frac{\partial^2\phi}{\partial x^2}\right|_{J,i} \tag{30}$$

where NV is the number of the surrounding triangular cells.

The second derivatives are used to determine the proper element sizes, h_i, $i = 1, 2$ in the two principal directions using condition,

$$h_i^2\lambda_i = h_{\min}^2\lambda_{\max} = \text{constant} \tag{31}$$

where λ_i, $i = 1, 2$ is the second derivatives of the unknown quantity in the two principal directions of the element considered. $\lambda_{\max} = \max\,(|(\partial^2\phi)/(\partial X^2)|, |(\partial^2\phi)/(\partial Y^2)|)$ is the maximum principal quantity for the entire model.

Based on the above condition, the element sizes are generated according to the given minimum element size $h_{\min}$. Specifying too small $h_{\min}$ may result in a model with an excessive number of elements. On the other hand, specifying too large $h_{\min}$ may result in an inadequate solution accuracy. These factors must be considered prior to generating a new mesh.

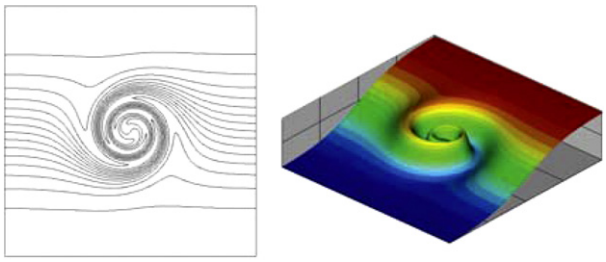

(a) 2D contour plot (b) 3D contour plot

Fig. 1. Exact solution of the mixing of hot with cold front. (a) 2D contour plot and (b) 3D contour plot.

5. Numerical examples

To evaluate the performance of the finite volume element method and to demonstrate the solution improvement after combining it with the adaptive meshing technique, five examples of pure-convection, convection-diffusion, convection-reaction and diffusion-reaction problems are performed. These examples are: (1) mixing of hot with cold front, (2) boundary layer flow, (3) oblique inflow convection-reaction, (4) corner layer problem, and (5) triangular wave flow problem.

5.1. Mixing of hot with cold front

The first example is a pure-convection problem of a mixing of hot with cold front [16]. The computational domain is $\Omega = (-4, 4) \times (-4, 4)$ and an initially straight frontal zone is given by,

$$\phi_0(\vec{x}) = -\tanh\left(\frac{y}{2}\right) \tag{32}$$

the velocity field is defined as,

$$\vec{v} = -\frac{y}{r}\frac{f_t}{f_{\max}}\vec{i} + \frac{x}{r}\frac{f_t}{f_{\max}}\vec{j} \tag{33}$$

where $r \equiv \sqrt{x^2 + y^2}$ is the distance from the origin of the coordinate system, $f_{\max} = 0.385$ is the maximum tangential velocity, and $f_t = (\tanh(r))/(\cosh^2(r))$. The problem is examined until the final time step is equal to 4. The exact solution is shown by the two- and three-dimensional contour plots in Fig. 1(a) and (b).

The computation is initially performed by using an unstructured mesh consisting of 884 uniform triangular cells. The initial and adaptive meshes with their computed solutions at the final time are shown by the two- and three-dimensional contour plots in Fig. 2(a)–(d), respectively. The element size used in the initial mesh is 0.4. The maximum and minimum element sizes of the third adaptive mesh are 1.0 and 0.004, respectively. The figures show that spurious oscillations decrease as the meshes are refined. The exact and computed solutions obtained from the third adaptive mesh are found to be good agreement.

5.2. Boundary layer flow

The second example is a convection-diffusion problem for determining the behavior of the boundary layer flow in a square domain $\Omega = (0, 1) \times (0, 1)$ [2]. The initial condition $\phi_0(\vec{x})$ is set to be zero and the velocity field is given by $\vec{v} = 1\vec{i}$. The small diffusion coefficient is specified as $\epsilon = 10^{-10}$ with the source term of $q = 1$.

The test case is performed until the final time step is equal to 2. The computation starts from using an unstructured mesh with 884 uniform triangular cells (20 cells along each boundary). Fig. 3(a)–(d) show the initial and adaptive meshes with their computed solutions at the final time by using the three-dimensional contour plots. The maximum and minimum element sizes of the third adaptive mesh are 0.1 and 0.002. Oscillation of the solution obtained from the coarse initial mesh occurs along the edge of the profile. This oscillation disappears after the second mesh adaptation.

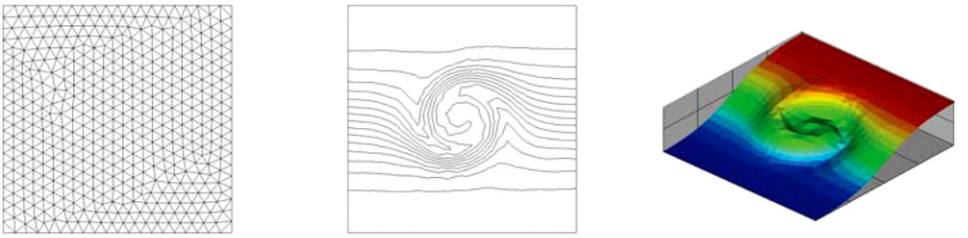

(a) Initial mesh and its solution

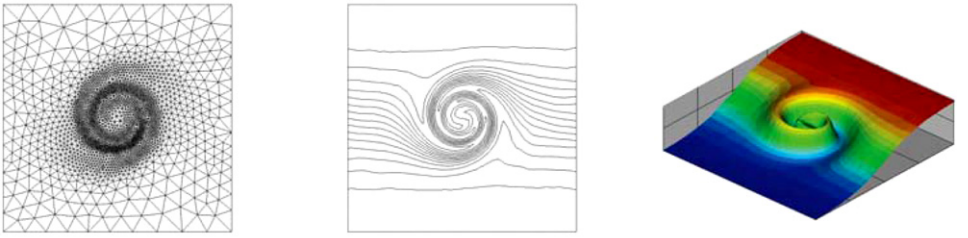

(b) First adaptive mesh and its solution

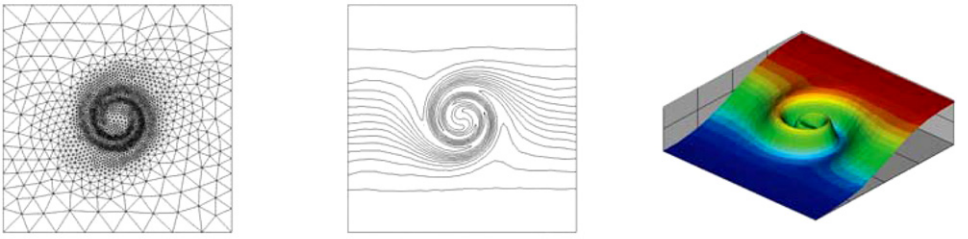

(c) Second adaptive mesh and its solution

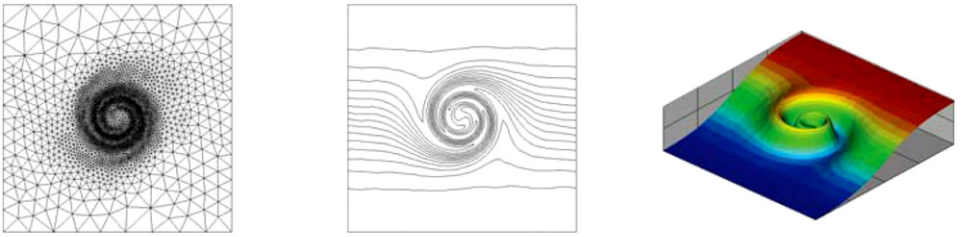

(d) Third adaptive mesh and its solution

Fig. 2. Adaptive meshes and their computed solutions for the mixing of hot with cold front. (a) Initial mesh and its solution, (b) first adaptive mesh and its solution, (c) second adaptive mesh and its solution, and (d) third adaptive mesh and its solution.

5.3. *Oblique inflow convection-reaction*

The third example is an oblique inflow convection-reaction problem [16]. The computational domain is a unit square of $\Omega = (0, 1) \times (0, 1)$, and the initial condition $\phi_0(\vec{x})$ is set to be zero. The source term, q, is given as a constant of 1. The steady velocity field is given in the form,

$$\vec{v} = V \cos\left(\frac{\pi}{3}\right)\vec{i} + V \sin\left(\frac{\pi}{3}\right)\vec{j} \tag{34}$$

Two different cases have been considered corresponding to dominant convection and reaction, respectively. These cases are:

(a) $V = 1.0$, $\kappa = 10^{-4}$ for convection-dominated problem, and

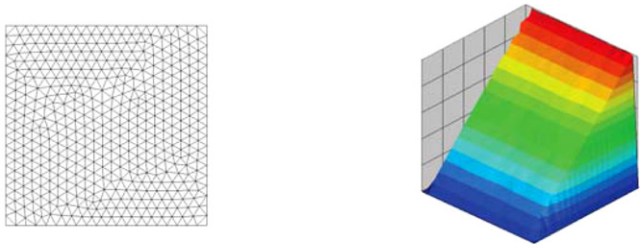

(a) Initial mesh and its solution

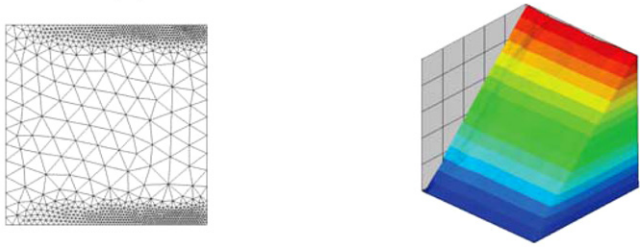

(b) First adaptive mesh and its solution

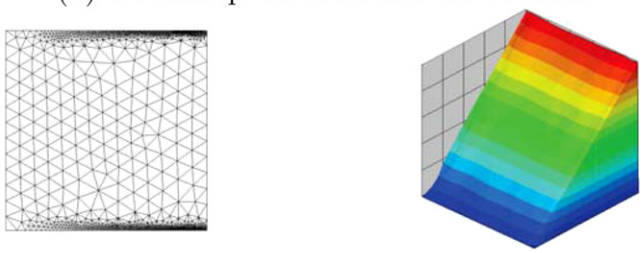

(c) Second adaptive mesh and its solution

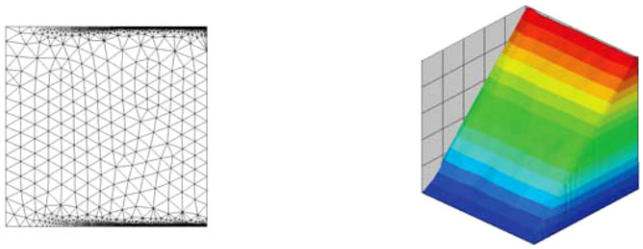

(d) Third adaptive mesh and its solution

Fig. 3. Adaptive meshes and their computed solutions of the boundary layer flow. (a) Initial mesh and its solution, (b) first adaptive mesh and its solution, (c) second adaptive mesh and its solution, and (d) third adaptive mesh and its solution.

(b) $V = 10^{-4}$, $\kappa = 1.0$ for reaction-dominated problem

The computation starts from using the same initial unstructured mesh as shown in the previous example. The initial and adaptive meshes with their corresponding steady-state solutions for case (a) are shown in Fig. 4(a)–(d), respectively. The analysis is performed until the final time step is equal to 2. With such a small reaction effect, the solution profile flows across the domain with an increasing amount of its height until it approaches the outflow boundaries. The oscillation occurs along the fronts of the profile from the use of the coarse initial mesh and diminishes after the second mesh adaptation. For case (b) where the reaction is dominated, the solution profile also flows across the domain with an increasing amount of its uniform height throughout the domain. This latter case is performed until the final time step is equal to 1. Fig. 5(a)–(d) show the initial and adaptive meshes with their corresponding solutions at the final time by using three-dimensional contour plots. Spurious oscillations occur along the profile fronts because of the coarse mesh. Such oscillations disappear after the meshes are adapted with small elements along the fronts of the profiles.

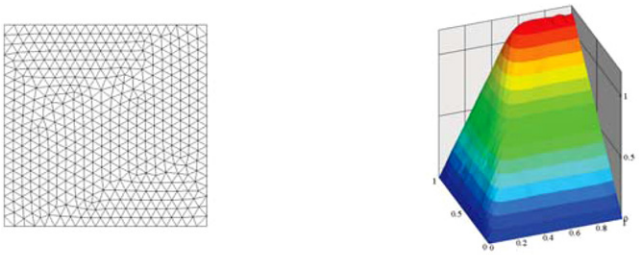

(a) Initial mesh and its solution

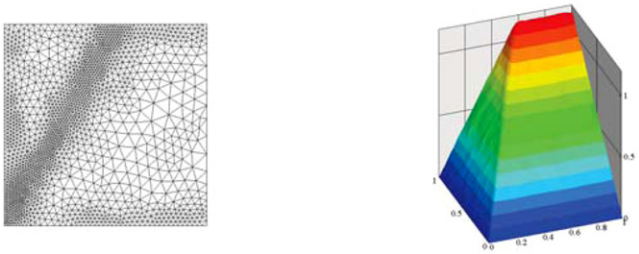

(b) First adaptive mesh and its solution

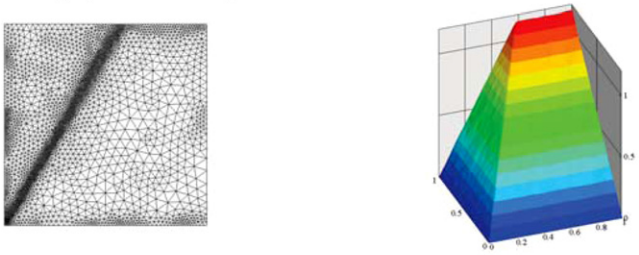

(c) Second adaptive mesh and its solution

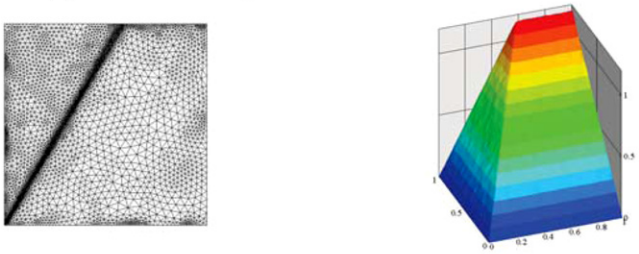

(d) Third adaptive mesh and its solution

Fig. 4. Adaptive meshes and their computed solutions of the oblique inflow convection-reaction (convection-dominated) problem. (a) Initial mesh and its solution, (b) first adaptive mesh and its solution, (c) second adaptive mesh and its solution, and (d) third adaptive mesh and its solution.

5.4. Corner layer problem

The fourth example is a singularly perturbed diffusion-reaction problem [18]. The computational domain is a unit square of $\Omega = (0, 1) \times (0, 1)$. The initial condition, $\phi_0(\vec{x})$, and the Dirichet boundary condition, $\phi(\vec{x})$, are prescribed as zero. The source term is given by,

$$q = 20\left(x^2 + y^2\right) + 4 \tag{35}$$

The diffusion coefficient is specified as $\epsilon = 10^{-3}$, and the reaction coefficient, κ, is set to be 2. This example is performed until the final time step is equal to 5. The solution profile exhibits very sharp boundary layer along the sides $x = 1$and $y = 1$. If the meshes in these regions are not fine enough, oscillated solution may occur along these boundaries, especially

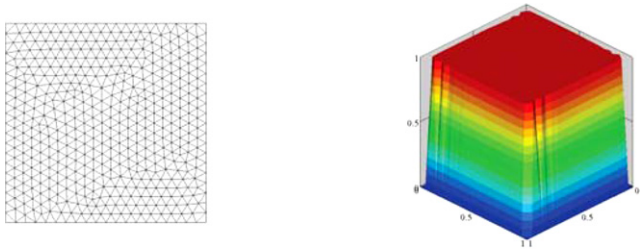

(a) Initial mesh and its solution

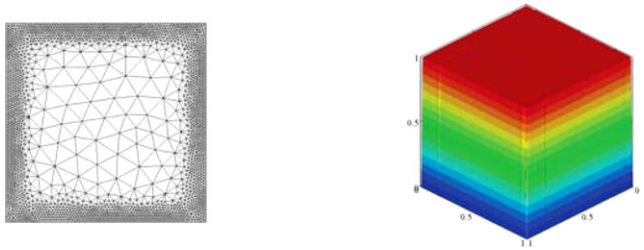

(b) First adaptive mesh and its solution

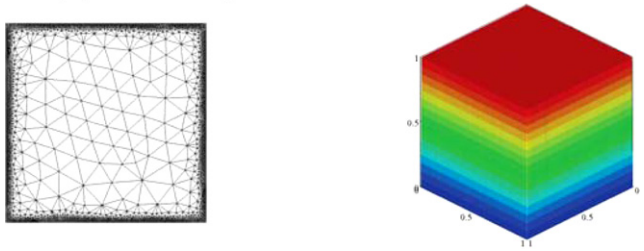

(c) Second adaptive mesh and its solution

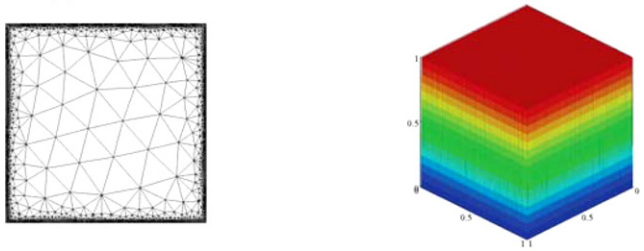

(d) Third adaptive mesh and its solution

Fig. 5. Adaptive meshes and their computed solutions of the oblique inflow convection-reaction (reaction-dominated) problem. (a) Initial mesh and its solution, (b) first adaptive mesh and its solution, (c) second adaptive mesh and its solution, and (d) third adaptive mesh and its solution.

at the corner point (1, 1). In order to help suppressing such oscillation, the Barth and Jespersen limiter function [1] is imposed as follows:

$$\alpha_{\Omega_i}^{BJ} = \min_{\forall \Gamma_{ij} \in \partial\Omega_i} \begin{cases} \dfrac{\phi_i^{\max} - \phi_i^n}{\phi_{ij}^{n+1/2} - \phi_i^n}, & \phi_{ij}^{n+1/2} > \phi_i^{\max} \\ \dfrac{\phi_i^{\min} - \phi_i^n}{\phi_{ij}^{n+1/2} - \phi_i^n}, & \phi_{ij}^{n+1/2} < \phi_i^{\min} \\ 1, & \text{otherwise} \end{cases} \tag{36}$$

where $\phi_i^{\max} \equiv \max_{\forall \Gamma_{ij} \in \partial\Omega_i}(\phi_i, \phi_j)$, (37a)

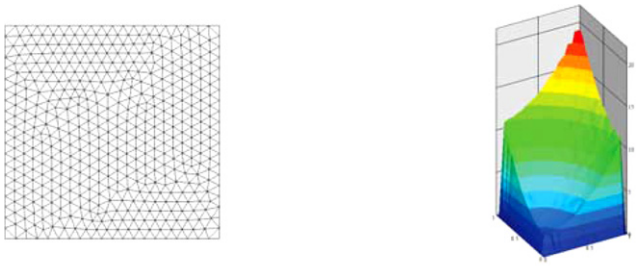

(a) Initial mesh and its solution

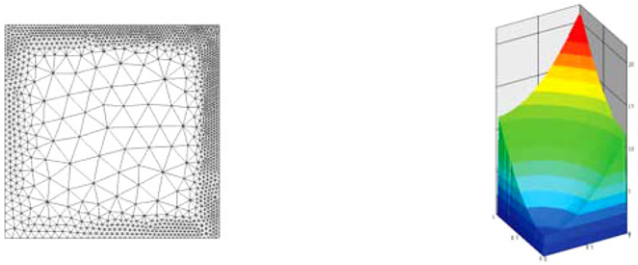

(b) First adaptive mesh and its solution

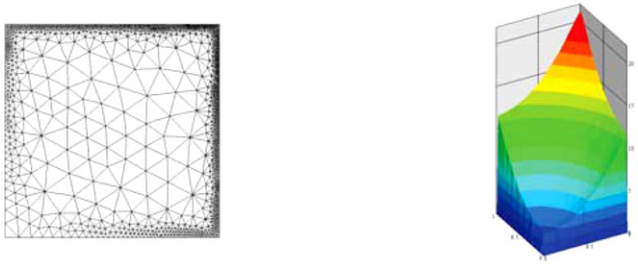

(c) Second adaptive mesh and its solution

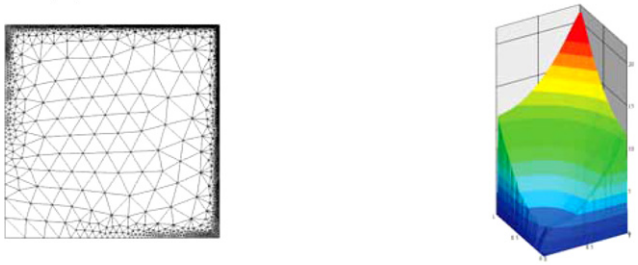

(d) Third adaptive mesh and its solution

Fig. 6. Adaptive meshes and their computed solutions of the corner layer problem. (a) Initial mesh and its solution, (b) first adaptive mesh and its solution, (c) second adaptive mesh and its solution, and (d) Third adaptive mesh and its solution.

$$\text{and} \qquad \phi_i^{\min} \equiv \min_{\forall \Gamma_{ij} \in \partial\Omega_i} (\phi_i, \phi_j) \tag{37b}$$

The computation is initially performed by using an unstructured mesh with 884 uniform triangular cells (20 cells along each boundary). As the meshes are adapted with the computed solutions, small element sizes are generated in the region of high solution gradients along the boundary sides $x = 1$ and $y = 1$. Fig. 6(a)–(d) show the initial and adaptive meshes with their corresponding solutions at the final time. The computed solution obtained from the initial mesh shows some oscillations without overshooting along the boundary. Oscillations decrease as the meshes are adapted with the solutions.

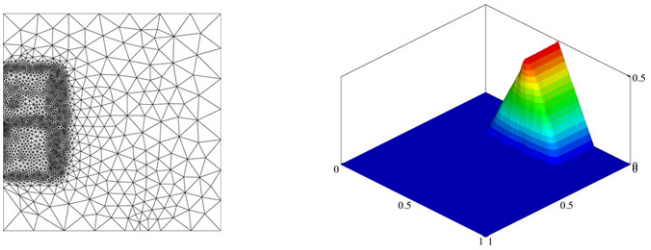

(a) Adaptive mesh and its solution at t = 5

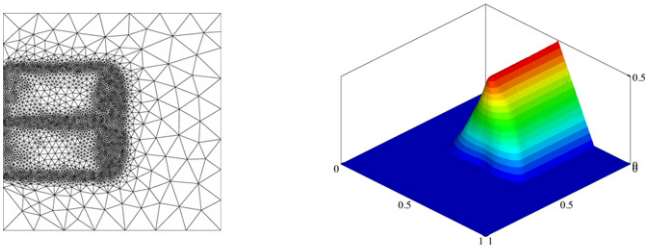

(b) Adaptive mesh and its solution at t = 10

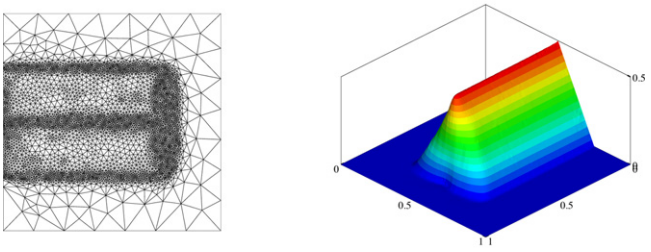

(c) Adaptive mesh and its solution at t = 15

Fig. 7. Adaptive meshes and their computed solutions of triangular wave flow problem. (a) Adaptive mesh and its solution at $t = 5$, (b) adaptive mesh and its solution at $t = 10$, and (c) adaptive mesh and its solution at $t = 15$.

5.5. *Triangular wave flow problem*

The last example is the pure-convection of triangular wave flow problem. The computational domain is a unit square of $\Omega = (0, 1) \times (0, 1)$. The initial condition, $\phi_0(\vec{x})$ is set to be zero. The boundary conditions are prescribed by,

$$\phi(0, y) = \begin{cases} 2(y - 0.25), & 0.25 \leq y < 0.50 \\ 2(0.75 - y), & 0.50 \leq y \leq 0.75 \\ 0, & \text{otherwise} \end{cases} \tag{38}$$

The velocity field is given by $\vec{v} = 0.05\vec{i}$. This example is used to evaluate the performance of the method when the adaptive meshes and their solutions vary with time. Fig. 7(a)–(c) show the adaptive meshes and their corresponding solutions at time $t = 5$, 10, and 15, respectively. These figures show that refined meshes are generated along the edges and profile front to capture high solutions gradients.

6. Conclusion

This paper presents a combination of an adaptive meshing technique and the finite volume element method for solving the unsteady convection-diffusion-reaction equation by using unstructured triangular cells. Theoretical formulation of the proposed method and the concept of adaptive meshing technique were explained. The finite volume method was applied to discretize the convection-diffusion-reaction equation and the weighted residuals concept of the finite element

method was implemented to estimate the gradient quantities at cell faces. Second-order accuracy in both space and time are achieved by applying the Taylor's series expansion along the local characteristic lines. The adaptive meshing technique generates small clustered elements in the regions of high solution gradients to increase the solution accuracy. Larger elements are generated in the other regions to reduce the computational time and computer memory. Five test cases were used to evaluate performance of the combined adaptive meshing and the finite volume element method. Results show that the combined method provides improved solution accuracy with the adaptive meshes.

Acknowledgement

The authors would like to thank the Office of Higher Education Commission, the Thailand Research Fund, and the National Metal, Materials Technology Center and Chulalongkorn University for supporting this research work.

References

[1] T. Barth, M. Ohlberger, Encyclopedia of Computational Mechanics Volume 1: Fundamentals, John Wiley and Sons, 2004.
[2] E.G.D. Carmo, G.B. Alvarez, A new stabilized finite element formulation for scalar convection-diffusion problems: the streamline and approximate upwind/Petrov–Galerkin method, Comput. Meth. Appl. Mech. Eng. 192 (2003) 3379–3396.
[3] E.G.D. Carmo, G.B. Alvarez, F.A. Rochinha, A.F.D. Loula, Galerkin projected residual method applied to diffusion-reaction problems, Comput. Meth. Appl. Mech. Eng. 197 (2008) 4559–4570.
[4] R. Codina, Comparison of some finite element methods for solving the diffusion-convection-reaction equation, Comput. Meth. Appl. Mech. Eng. 156 (1998) 185–210.
[5] P. Dechaumphai, Adaptive finite element technique for heat transfer problems, J. Energ. Heat Mass Transfer 17 (1995) 87–94.
[6] P. Dechaumphai, Finite Element Method: Fundamentals and Applications, Alpha Science Intl. Ltd, 2010.
[7] F. Ilinca, J.F. Hetu, A new stabilized finite element method for reaction-diffusion problems: the source-stabilized Petrov–Galerkin method, Int. J. Num. Meth. Eng. 75 (2008) 1607–1630.
[8] H. Jasak, H.G. Weller, A.D. Gosman, High resolution NVD differencing scheme for arbitrarily unstructured meshes, Int. J. Num. Meth. Fluids 31 (1999) 431–449.
[9] A. Kruganov, E. Tadmor, New high-resolution central schemes for nonlinear conservation laws and convection-diffusion equations, J. Comput. Phys. 160 (2000) 241–282.
[10] S. Lamine, M.G. Edwards, High-resolution convection schemes for flow in porous media on highly distorted unstructured grids, Int. J. Num. Meth. Eng. 76 (2008) 1139–1158.
[11] R.J. Leveque, Finite Volume Methods for Hyperbolic Problems, 3rd edition, Cambridge University Press, 2005.
[12] W. Limtrakarn, P. Dechaumphai, High-speed compressible flow analysis by adaptive cell-centered finite elements, J. Energ. Heat Mass Transfer 24 (2002) 141–162.
[13] A. Malatip, N. Wansophark, P. Dechaumphai, Combined streamline upwind Petrov Galerkin method and segregated finite element algorithm for conjugated heat transfer problems, J. Mech. Sci. Technol. 20 (2009) 1741–1752.
[14] J. Peraire, J. Peiro, L. Formaggia, K. Morgan, O.C. Zienkiewica, Finite element Euler computations in three dimensions, Int. J. Num. Meth. Fluids 26 (1995) 2135–2159.
[15] J. Peraire, M. Vahjdati, K. Morgan, O.C. Zienkiewicz, Adaptive remeshing for compressible flow computation, J. Comput. Phys. 72 (1987) 449–466.
[16] S. Phongthanapanich, P. Dechaumphai, A characteristic-based finite volume element method for convection-diffusion-reaction equation, Trans. Can. Soc. Mech. Eng. 32 (2008) 549–559.
[17] S. Phongthanapanich, P. Dechaumphai, Combined finite volume and finite element method for convection-diffusion-reaction equation, J. Mech. Sci. Technol. 23 (2009) 790–801.
[18] S. Phongthanapanich, P. Dechaumphai, Combined finite volume element method for singularly perturbed reaction-diffusion problems, Appl. Math. Comput. 209 (2009) 177–185.
[19] J. Principe, R. Codina, On the stabilization parameter in the subgrid scale approximation of scalar convection-diffusion-reaction equations on distorted meshes, Comput. Meth. Appl. Mech. Eng. 199 (2010) 1386–1402.
[20] H. Wang, J. Liu, Development of CFL-free explicit schemes for multidimensional advection-reaction equations, SIAM J. Sci. Comput. 23 (2001) 1418–1438.
[21] O.C. Zienkiewicz, R. Codina, A general algorithm for compressible and incompressible flow – part I. The split, characteristic-based scheme, Int. J. Num. Meth. Fluids 20 (1995) 869–885.
[22] O.C. Zienkiewicz, R.L. Taylor, The Finite Element Method Volume 3: Fluid Dynamics, 5th edition, Butterworth-Heinemann, 2000.